Microchimica Acta (2024) 191:378
https://doi.org/10.1007/s00604-024-06471-5

ORIGINAL PAPER

Hg^{2+}-enhanced oxidase-like activity of platinum nanoparticles immobilized on porphyrin-based porous organic polymer for the colorimetric detection and removal of Hg^{2+}

Liqin Zhu[1] · Congcong Lou[1] · Xiaomei Zhang[1] · Fei Yang[1]

Received: 28 February 2024 / Accepted: 27 May 2024 / Published online: 9 June 2024

Abstract

Porphyrin-based porous organic polymer (POP) with uniformly immobilized platinum nanoparticles (Pt NPs) were designed and synthesized, and it was demonstrated that such nanocomposites (Pt/POP) have oxidase-like activity. Surprisingly, Hg^{2+} significantly enhanced the oxidase-like activity of Pt/POP. The enhancement was attributed to the capture of Hg^{2+} by the thioether group in Pt/POP and the subsequent redox reaction of Hg^{2+} with Pt NPs, accelerating the electron transfer. In the presence of Hg^{2+}, Pt/POP catalyzed the colorless 3,3',5,5'-tetramethylbenzidine (TMB) to turn blue rapidly and changed its absorbance at 652 nm. Based on this, a fast-response colorimetric sensor was constructed for the sensitive detection of Hg^{2+} with a linear range of 0.2–50 μM and a detection limit of 36.5 nM. Importantly, Pt/POP can be used as an adsorbent for the efficient removal of Hg^{2+} with a removal efficiency as high as 99.4%. This work provides a valuable strategy for colorimetric detection and efficient removal of Hg^{2+}.

Keywords Porous organic polymer · Oxidase-like activity · Detection of Hg^{2+} · Colorimetric sensor · Removal of Hg^{2+}

Introduction

Hg^{2+} is a highly toxic and non-biodegradable heavy metal ion that produces harmful effects on a wide range of tissues and organs [1–3]. Atmospheric deposition and industrial emissions increase mercury deposition in lakes and soils [4–6], and Hg^{2+} is biologically taken up and amplified [7, 8], causing ecological and human health problems. Among various analytical methods, including atomic absorption spectrometry, inductively coupled plasma mass spectrometry, electrochemistry, fluorescence spectroscopy, and colorimetric methods, colorimetric methods have become increasingly popular because of their simplicity, low cost, and rapid and naked-eye-visible color change. They have been widely used for the detection of heavy metal ions [9, 10], small molecules [11], and organic pollutants [12], among others.

Currently, nanomaterials play a crucial role in the rapid detection and effective removal of Hg^{2+}. On the one hand, composites based on noble metal nanoparticles provide a sensitive method for detecting Hg^{2+}. For example, Shi et al. developed MXene/DNA/Pt nanocomposites with peroxidase-like activity, which enabled quantitative detection of Hg^{2+} due to the inhibition of the peroxidase-like activity of the nano-enzymes by Hg^{2+} [13]. Li et al. proposed a novel targeting COFs with sulfur-liganded Au atoms based on Tz-COF@Au NPs with Hg^{2+} activated peroxidase-like activity and developed a strategy to detect Hg^{2+} [14]. On the other hand, various functionalized nanomaterials such as metal–organic frameworks [15], covalent organic frameworks [16], porous organic materials [17, 18], and carbon nanotubes [19] have been used to remove Hg^{2+} from water. However, due to the high chemical activity and low affinity of Hg^{2+}, most of the nanomaterials used for Hg^{2+} detection adsorb only a tiny amount of Hg^{2+} [20, 21], and some of them do not even remove Hg^{2+} effectively [22–24]. Therefore, designing and developing bifunctional nanomaterials that can detect Hg^{2+} with high sensitivity and rapidity and adsorb a large amount of Hg^{2+} remains a significant challenge.

✉ Fei Yang
yangfei@sdu.edu.cn

[1] School of Pharmaceutical Sciences, School of Chemistry and Chemical Engineering, Shandong University, Jinan 250000, Shandong, China

As emerging porous materials, porous organic polymers (POPs) have attracted much attention in storage, catalysis, and adsorption due to their high specific surface area, multilevel pore structure, and customizable units. In previous reports, Hg^{2+} can enhance or inhibit the catalytic activity of noble metal nanomaterials (Au, Ag, Pt, etc.) [25, 26], and noble metal-based catalysts have been developed as colorimetric sensors for detecting Hg^{2+}. Remarkably, uniformly immobilized Pt NPs usually have excellent catalytic properties [27, 28]. Strong interactions between thioether groups (-S-R) and Pt NPs have been found [29], and introducing -S-R in porous materials to control the distribution of Pt NPs is a new idea. In addition, the high affinity of -S-R for Hg^{2+} makes it easy to trap Hg^{2+} [30], and the synergistic interaction between the thioether-functionalized POPs and the ordered pore structure results in a high mercury adsorption capacity [31]. Thus, the introduction of -S-R into porous materials not only homogeneously immobilizes Pt NPs but also shows excellent potential for Hg^{2+} removal.

Here, we prepared POP by one-step condensation of pyrrole and 2,5-bis (methylthio) terephthalaldehyde (BMTA). Then, Pt/POP was prepared by in situ loading of Pt NPs into the POP material using a thermal reduction method. Pt/POP alone exhibited weak oxidase-like activity, but the oxidase-like activity was significantly elevated when coexisting with Hg^{2+}. The Pt/POP-Hg^{2+} system catalyzed the chromogenic reaction of TMB, and based on that, a colorimetric method was developed to detect Hg^{2+}. Notably, the proposed colorimetric sensor has the advantages of good selectivity, simplicity, and rapidity in detecting Hg^{2+} and has been successfully applied to detecting Hg^{2+} in industrial wastewater. Meanwhile, Pt/POP can remove Hg^{2+} from aqueous solutions.

Experimental section

Materials and instruments

2,5-dibromo-p-benzaldehyde, propionic acid, pyrrole, sodium thiomethoxide ($NaSCH_3$), isopropanol (IPA), and 1,4-benzoquinone (PBQ) were purchased from Anhui Zesheng Technology Co., Ltd. (Anhui, China). Ethylenediaminetetraacetic acid disodium salt (EDTA-2Na) was purchased from Bide Pharmatech Ltd. (Shanghai, China). Histidine (HD) was purchased from Shanghai Dipper Biotechnology Co., Ltd. (Shanghai, China). 3,3',5,5'-tetramethylbenzidine (TMB) was obtained from Aladdin Co., Ltd. (Shanghai, China).

UV-8000X UV–visible spectrophotometer (Shanghai, China) obtained the UV–visible absorption spectrum. Scanning electron microscopy (SEM) images were performed on a Hitachi SU-4800 (Japan) scanning electron microscopy. Transmission electron microscope (TEM) images were obtained on a JEOL JEM-1011 transmission electron microscope with an accelerating voltage of 100 kV. Powder X-ray diffraction (XRD) patterns were recorded on a Bruker D8 Advanced X-ray diffractometer. X-ray photoelectron spectroscopy (XPS) data was collected on Thermo Scientific K-Alpha.

Synthesis of Pt/POP nanocomposite

Details of the preparation of BMTA and POP were in Experiments S1 and S2. 10 mg POP and 30 mg PVP-K30 were added to a 20 mL glass vial, then 5 mL ethanol, 4.5 mL deionized water, and 0.5 mL K_2PtCl_6 (0.1 M) were added, mixed ultrasonically, and stirred for 3 h. The reaction was carried out under vigorous stirring at 80 ℃ for 3 h. The product was recovered by centrifugation and washed three times with a mixture of ethanol and water (1:1). The product was dried under vacuum at 60 ℃ for 24 h to obtain a black powder.

Determination of Hg^{2+}-enhanced oxidase-like activity

POP was used as a control to investigate the enhancing effect of Hg^{2+} on the oxidase-like activity of Pt/POP. Pt/POP solution (200 µL, 25 µg/mL), Hg^{2+} (200 µL, 10 µM), and TMB (200 µL, 100 µM) were added into NaAc-HAc buffer solution (1.4 mL, pH 4). The mixed system was reacted at room temperature for 1 min, and then the absorbance was scanned by a UV–visible spectrophotometer at 652 nm. The effects of Pt/POP solution concentration, Hg^{2+} concentration, TMB concentration, pH, temperature, and reaction time on the enhancement of Pt/POP oxidase activity by Hg^{2+} were also evaluated.

Colorimetric detection of Hg^{2+}

Pt/POP solution (200 µL, 25 µg/mL) and TMB (200 µL, 80 µM) were added to NaAc-HAc buffer (1.6 mL, pH = 4), and the reaction was carried out at room temperature for 2 min, and the absorbance value at 652 nm was measured (A_0). Then, the absorbance values of different concentrations of Hg^{2+} were measured under the same conditions (A_1). The relationship between ΔA (A_1-A_0) and Hg^{2+} concentration was plotted. In addition, the catalytic performance of Pt/POP in different cations was explored to evaluate the selectivity and sensitivity of Pt/POP to Hg^{2+}.

Removal of Hg^{2+}

The removal efficiency of Pt/POP as an adsorbent for Hg^{2+} from aqueous solutions was investigated. The pH of the

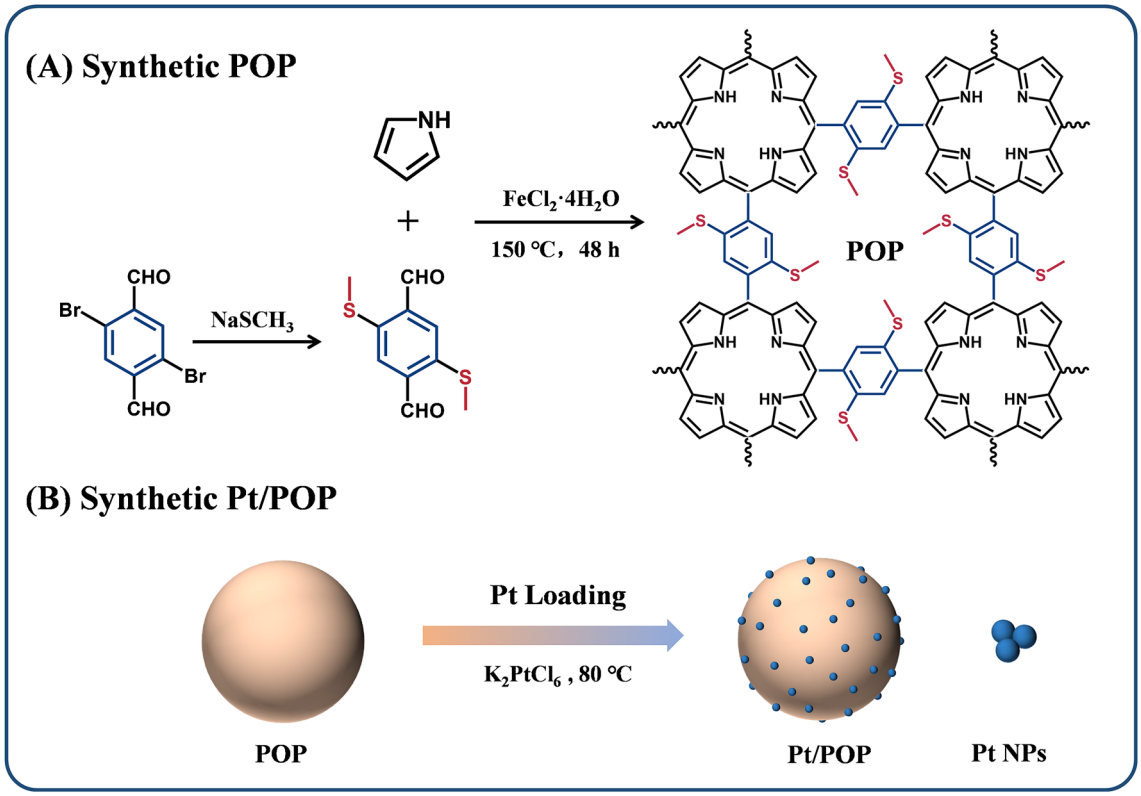

Scheme 1 **A** Synthesis of POP. **B** Preparation of Pt/POP by thermal reduction

aqueous Hg^{2+} solution was adjusted to 7 with HNO_3 and NaOH, then 1 mg of Pt/POP was dispersed into 5 mL of aqueous Hg^{2+} solution (60, 70, 80, 90, and 100 ppm), and the mixture was shaken for 6 h. The supernatant was separated by centrifugation, the residual Pt/POP was filtered, and the concentration of residual Hg^{2+} was determined by inductively coupled plasma-optical emission spectrometry (ICP-OES).

Results and discussion

Characterization of Pt/POP

Briefly, POP was prepared by one-step condensation of pyrrole and BMTA (Scheme 1A), and the two -S-R functional groups of BMTA bind strongly to the metal NPs, facilitating the formation of uniformly distributed Pt NPs in POP materials. Then, K_2PtCl_6 was used as a precursor of Pt, and Pt NPs were immobilized into POP materials using the thermal reduction method (Scheme 1B).

The morphological characterization of POP and Pt/POP was performed using transmission electron microscopy (TEM) and scanning electron microscopy (SEM). As shown in Fig. 1A, the prepared POP presented a uniform spherical shape with an average size of 200 nm. The TEM images of Pt/POP showed (Fig. 1B-C) that the ultra-small Pt NPs were uniformly distributed in the POP material, and the average particle size of the Pt NPs was 2.7 ± 0.5 nm (inset in Fig. 1D). The Pt lattice was observed from the inset of Fig. 1E with a lattice spacing of 0.225 nm in the Pt (111) plane [32]. After loading Pt NPs, the surface of POP became rough (Fig. 1F). The energy dispersive X-ray spectroscopy (EDS) images showed that the C, N, S, and Pt elements were uniformly distributed on the Pt/POP (Fig. 1G). Due to the limitation of the EDS method, no Fe was detected in Pt/POP. Subsequently, further analysis by ICP-MS showed that the weight percentages of Pt and Fe in Pt/POP were 8.73% and 0.20%, respectively. From the EDS and ICP-MS results, Pt/POP is almost free of iron, but the addition of $FeCl_2$ plays a crucial role in the size and morphology of the material.

The FT-IR spectra of POP and Pt/POP were comprehensively compared (Fig. 2A). In the FT-IR spectrum of POP, the C = O stretching vibrational peak of BMTA (1688 cm^{-1}) almost disappeared, and the C-H stretching vibrational peak of methyl group (2918 cm^{-1}) appeared, indicating the successful preparation of POP. In addition, the characteristic peaks of Pt/POP were the same as those of POP, which stated that the structure of POP remained intact even when Pt NPs were formed. ^{13}C CP-MAS NMR spectra further

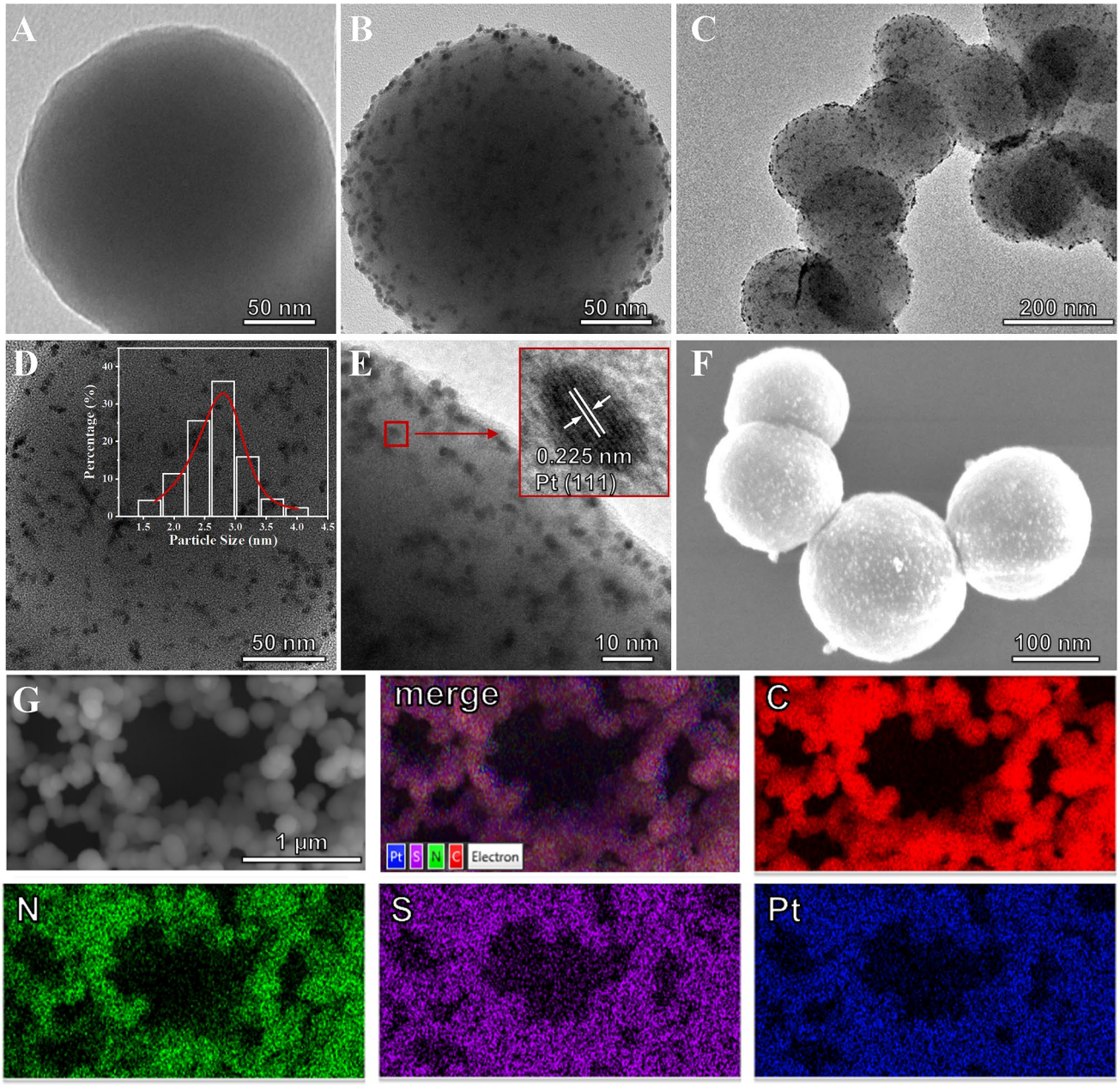

Fig. 1 TEM images of (**A**) POP and (**B**-**C**) Pt/POP. **D** HRTEM image of Pt/POP and the size distribution profile of Pt NPs (inset). **E** HRTEM image of Pt/POP and the lattice pattern of the loaded Pt NPs (inset). **F** SEM image of Pt/POP. **G** HAADF-STEM image of Pt/POP and the corresponding elemental mapping of C, N, S, and Pt

confirmed the successful synthesis of POP. As shown in Fig. S1, the strong peak at 13.2 ppm was associated with the carbon of the methylthio group [33], and the peaks at 100–150 ppm were attributed to the carbon of the benzene and porphyrin rings. As shown in Fig. 2B, a typical broad peak of POP (23.80°) appeared in the XRD plot of Pt/POP since POP is an amorphous polymer, while characteristic diffraction peaks were observed at 39.56°, 46.14°, and 67.08°, which can be attributed to the planar surfaces of the Pt nanocrystals at (111), (200), and (220).

The chemical composition of Pt/POP was investigated by X-ray photoelectron spectroscopy (XPS). The appearance of the Pt 4f signal in the XPS full-scan spectra of Pt/POP reconfirmed the successful growth of Pt NPs on the POP surface (Fig. 2C). The binding energies of the electrons in the Pt 4f orbitals were decomposed into Pt^0 and Pt^{2+} components, with peaks at 70.2 and 73.3 eV coming from Pt $4f_{7/2}$ and Pt $4f_{5/2}$ of Pt^0, respectively, and peaks at 71.7 and 74.8 eV corresponding to Pt $4f_{7/2}$ and Pt $4f_{5/2}$ of Pt^{2+}, respectively (Fig. 2D). The pore size distributions of POP

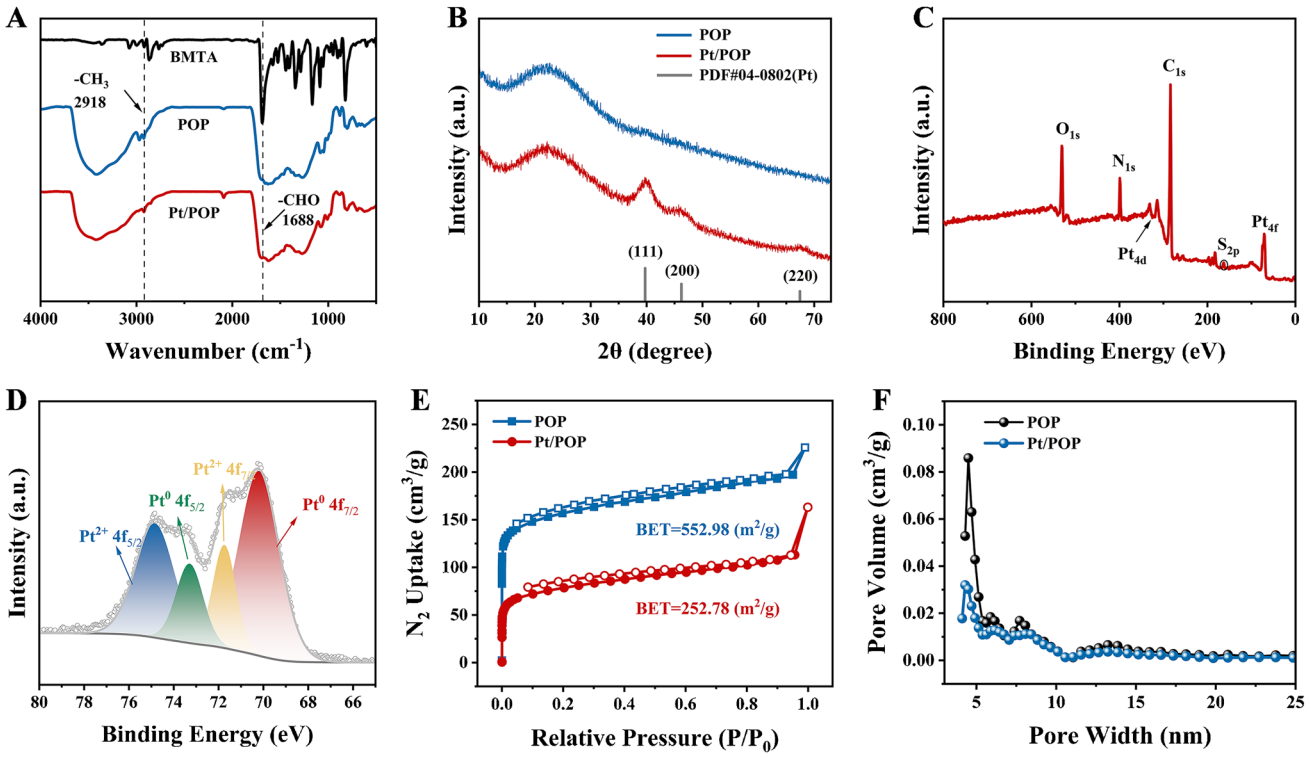

Fig. 2 **A** FT-IR spectra of BMTA, POP, and Pt/POP. **B** X-ray diffraction patterns of POP and Pt/POP. **C** XPS analysis of Pt/POP. **D** XPS spectrum for the Pt 4f species of Pt/POP. **E** Nitrogen adsorption and desorption isotherms of POP and Pt/POP. **F** Pore size distribution of POP and Pt/POP

and Pt/POP were analyzed by nitrogen adsorption–desorption isotherms (Fig. 2E-F). The BET-specific surface area of POP was 552.98 m^2/g, while that of Pt/POP was considerably reduced (252.78 m^2/g), which may be attributed to Pt NPs clogging the pores. The major pore diameters of POP and Pt/POP were concentrated at ~ 4.30 and ~ 4.49 nm. The pore volume of Pt/POP decreased significantly after the loading of Pt NPs, which indicated that some of the Pt NPs were located in the pores of POP. As shown in Fig. S2, the mass loss of both POP and Pt/POP did not exceed 20% when heated up to 300 °C, indicating both materials' good thermal stability.

Catalytic activity of Pt/POP

To investigate the oxidase-like catalytic properties of Pt/POP enhanced by Hg^{2+}, the absorbance at 652 nm was studied in different systems using TMB as substrate. As shown in Fig. 3A, no absorption peaks and color changes of ox-TMB were observed in the TMB or Hg^{2+} + TMB systems. The Pt/POP + TMB system showed weak absorption peaks and blue color, but when Pt/POP coexisted with Hg^{2+}, firm absorption peaks appeared at 652 nm, along with apparent blue color changes in the solution. It was found that the catalytic performance of Pt/POP with the addition of Hg^{2+} increased 16-fold compared with that of pure Pt/POP (Fig. 3B), confirming that the Pt/POP catalysts possessed excellent Hg^{2+}-enhanced oxidase-like activity. In addition, the oxidase-like activity of the Pt/POP-Hg^{2+} system was significantly increased by 11 times compared with that of the POP-Hg^{2+} system. It is evident that the introduction of Pt NPs accelerated the electron transfer and significantly enhanced the Hg^{2+}-enhanced oxidase-like activity of the materials. The possible reason is that Hg^{2+} binds to the -S-R group in Pt/POP and changes its surface properties. Then, Pt^0 undergoes a redox reaction with Hg^{2+}, accelerating the electron transfer and improving the catalytic performance of Pt/POP.

Next, the experimental conditions, such as Pt/POP concentration, time, pH, temperature, and TMB concentration, were optimized. As shown in Fig. 3C, when the Pt/POP concentration was 25 μg/mL, the absorbance at 652 nm showed an increasing trend and then stabilized at 120 s. In addition, the absorbance at 652 nm increased with increasing Hg^{2+} concentration and reached equilibrium at 120 s as the reaction progressed (Fig. 3D). As shown in Fig. 3E-F, the oxidase-like activity of Pt/POP-Hg^{2+} was optimal at pH 4 and 25 °C. Therefore, 25 μg/mL Pt/POP, reaction time of 120 s, buffer solution at pH 4, 25 °C, and 80 μM TMB (Fig. S3) were considered the best conditions for detecting Hg^{2+}.

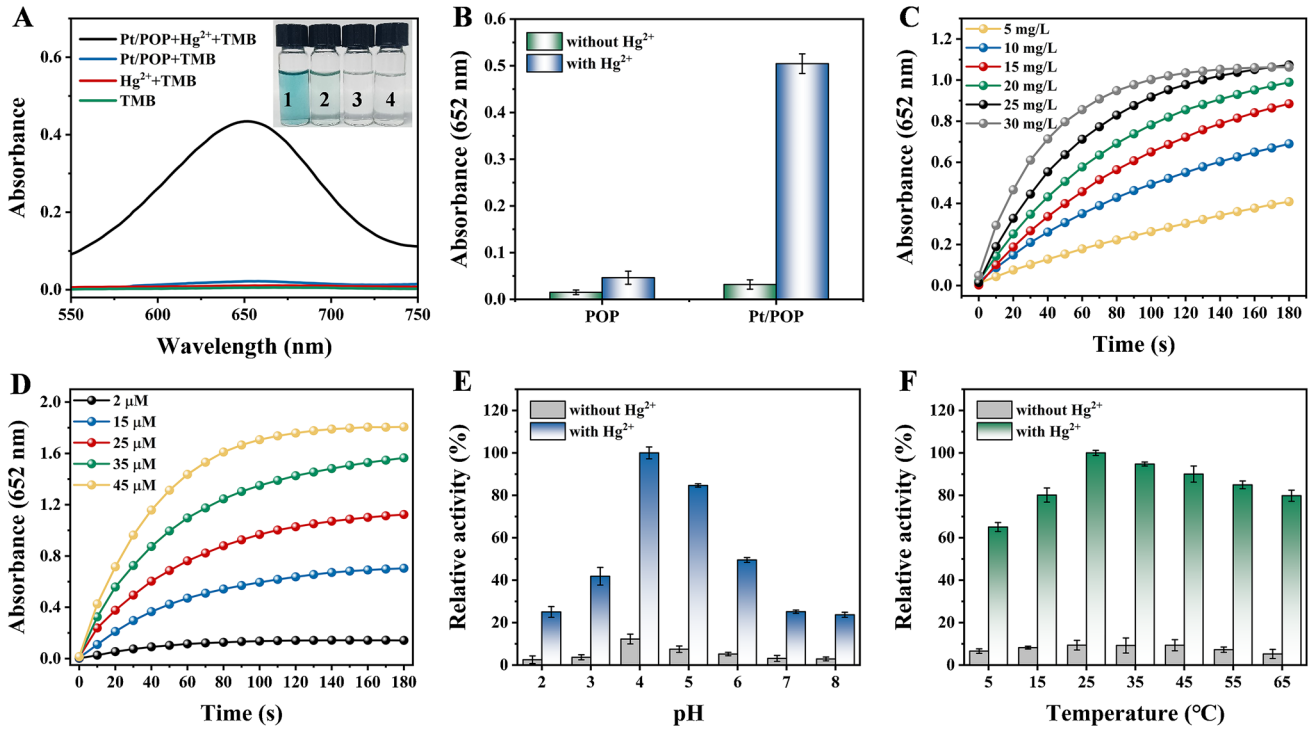

Fig. 3 **A** The UV–vis absorption spectra of different systems, Inset: Color change of Pt/POP + Hg^{2+} + TMB system (1), Pt/POP + TMB system (2), Hg^{2+} + TMB (3) and TMB (4). **B** Comparison of the Hg^{2+}-enhanced oxidase-like activity of POP and Pt/POP. **C** Variation of absorbance with time for different concentrations of Pt/POP. **D** Temporal variation of absorbance at 652 nm for the Pt/POP + Hg^{2+} + TMB system. Effect of (**E**) pH of buffer solution and (**F**) temperature on the oxidase-like activity of Pt/POP-Hg^{2+}

Kinetic experiments under added Hg^{2+} conditions analyzed the catalytic performance of Pt/POP. As shown in Fig. S4, $K_m = 0.0259$ mM and $V_{max} = 1.4 \times 10^{-4}$ mM/s were calculated using the Lineweaver-Menten equation (eq. S1). The K_m value of Pt/POP-Hg^{2+} was minimal, which indicated that Pt/POP had a good affinity with TMB in the presence of Hg^{2+}. In addition, the V_{max} value of Pt/POP was very high and the reaction speed was breakneck. Kinetic studies showed that the affinity of Pt/POP-Hg^{2+} for TMB was significantly better than that of other nanoenzymatic materials (Table S1).

The catalytic mechanism of Pt/POP

Free radical trapping experiments determined the catalytic process of Hg^{2+}-enhanced oxidase-like activity. To determine the reactive oxygen species (ROS), IPA, HD, PBQ, and EDTA-2Na were utilized as scavengers of hydroxyl radical (·OH), superoxide anion ($O_2 \cdot^-$), singlet oxygen ($^1O_2$) and hole (h^+), respectively. As shown in Fig. 4A and S5, IPA had a negligible effect on the system, indicating that the catalytic process did not produce ·OH. When PBQ was present in the system, the absorbance was slightly decreased, indicating that the system made a small amount of $O_2 \cdot^-$. However, the absorbance of the system in the presence of HD and EDTA-2Na decreased significantly, indicating that the Hg^{2+}-enhanced oxidase-like activity of Pt/POP originated from $^1O_2$ and h^+.

Then, the mechanism of Hg^{2+}-enhanced oxidase-like activity of Pt/POP was further investigated. To verify the binding of Pt/POP with Hg^{2+}, we analyzed the surface properties and chemical compositions of Pt/POP before and after Hg^{2+} treatment by XPS spectroscopy. Unsurprisingly, compared with the pristine Pt/POP, the complete XPS spectra of Pt/POP-Hg^{2+} exhibited new characteristic peaks corresponding to Hg 4f (Fig. 4B), indicating that Pt/POP can adsorb Hg^{2+}. It is reported that the -S-R functional group has a strong affinity for elemental mercury. After the treatment with Hg^{2+}, the C and N species in the high-resolution C 1 s and N 1 s remained almost unchanged (Fig. S6). In contrast, the S species in the high-resolution S 2p shifted significantly (Fig. 4C), the S $2p_{3/2}$ shifted from 162.05 to 162.55 eV, and the S $2p_{1/2}$ shifted from 163.10 to 163.50 eV, suggesting that there was a strong interaction between the S species and Hg^{2+} [34].

The characteristic peaks of high-resolution Pt 4f were decomposed into Pt^0 and Pt^{2+} components (Fig. 4D), and the relative contents of Pt^0 and Pt^{2+} were analyzed before and after Hg^{2+} treatment. As shown in Fig. 4F, the relative content of Pt^0 decreased to 44.3%, and that of Pt^{2+}

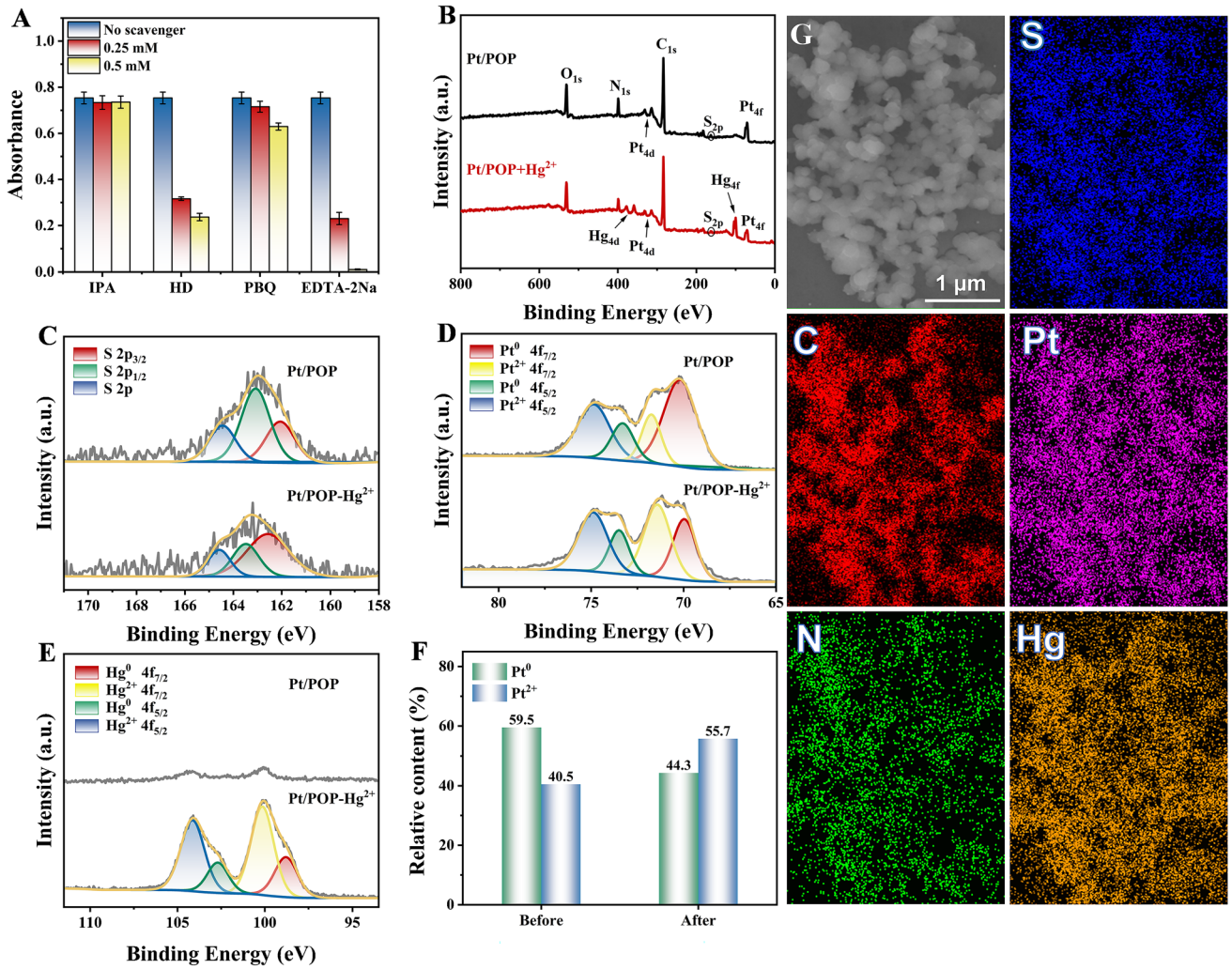

Fig. 4 **A** Inhibition of Pt/POP-Hg^{2+} + TMB system by different scavengers. **B** XPS spectra of Pt/POP before and after Hg^{2+} incubation. XPS spectra of Pt/POP before and after Hg^{2+} incubation with high-resolution (**C**) S 2p, (**D**) Pt 4f, and (**E**) Hg 4f. **F** Relative content of Pt^0 and Pt^{2+} in Pt/POP before and after Hg^{2+} incubation. **G** SEM image and elemental maps of Pt/POP after Hg^{2+} incubation

increased to 55.7%, indicating that the presence of Hg^{2+} accelerated the oxidation reaction. The high-resolution Hg 4f of Pt/POP-Hg^{2+} displayed two characteristic peaks belonging to Hg $4f_{7/2}$ and Hg $4f_{5/2}$ of Hg-S bonding, respectively (Fig. 4E), of which the peaks at 98.8 eV and 102.65 eV were related to Hg^0, suggesting that there is a process of reduction of Hg^{2+} to Hg^0 on the surface of Pt/POP, which may be similar to that of reduction of Hg^{2+} by Pt NP@UiO-66-NH_2 [35]. In addition, the presence of elemental mercury on the Hg^{2+}-treated Pt/POP surface was further verified by SEM and the corresponding elemental mapping analysis (Fig. 4G). In summary, the mechanism of the enhanced oxidase-like activity of Hg^{2+} may be that Hg^{2+} binds to the S elements in Pt/POP to form Hg-S bonds, which changes the surface properties of Pt/POP, and the interaction between Pt^0 and Hg^{2+} accelerates the electron transfer.

Colorimetric detection of Hg^{2+}

In the presence of Pt/POP, different concentrations of Hg^{2+} enhanced the color development reaction of TMB to various degrees. Therefore, a colorimetric platform for detecting Hg^{2+} was constructed based on the Hg^{2+}-enhanced oxidase-like activity of Pt/POP (Scheme 2). As shown in Fig. 5A, ΔA increased with increasing Hg^{2+} concentration and exhibited good linearity in the range of 0.2–50 μM, with a limit of detection of 36.5 nM calculated according to the 3σ/k rule, which is lower than most of the nanomaterials used for Hg^{2+} detection (Table S2). Next, the effects of other interfering ions on the oxidase-like activity of Pt/POP were investigated. As shown in Fig. 5B, the response intensity of Hg^{2+} at 652 nm was about 10 times higher than that of other interfering ions, and the solution containing Hg^{2+} showed a distinct blue color, which indicated that Pt/POP had good

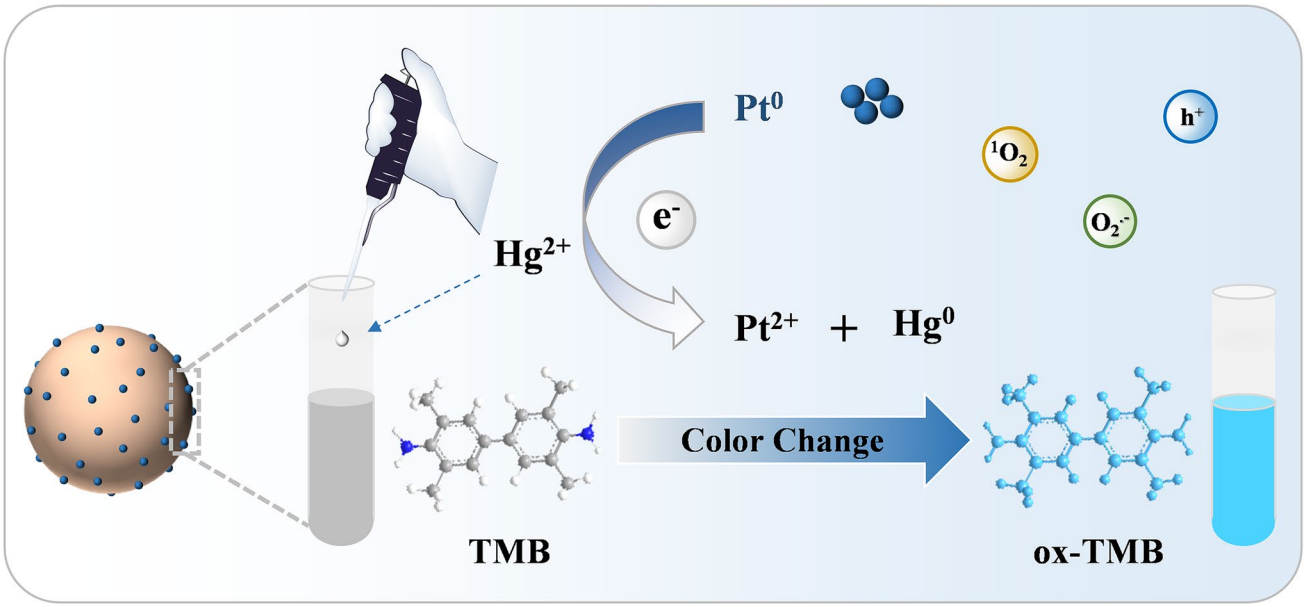

Scheme 2 Colorimetric detection of Hg^{2+} using Hg^{2+}-enhanced oxidase-like activity of Pt/POP

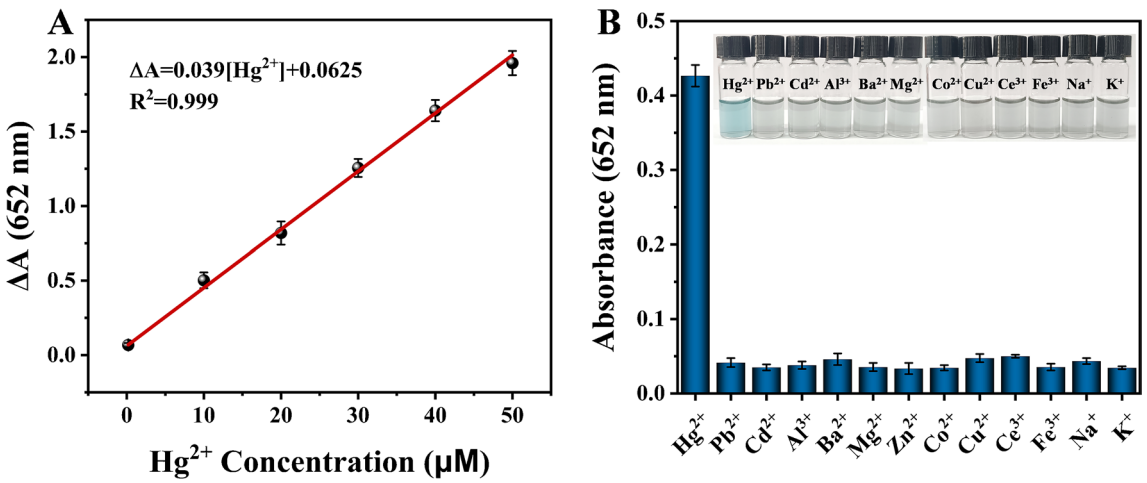

Fig. 5 **A** Linear calibration plot of Hg^{2+} at 652 nm ($\Delta A = A_1 - A_0$, A_0, and A_1 represent absorbance at 652 nm before and after adding Hg^{2+}, respectively). **B** Selectivity of detection of Hg^{2+} compared to other interfering substances

selectivity for Hg^{2+}. In addition, the catalytic activity of Pt/POP remained above 90% after two months of storage (Fig. S7).

The Pt/POP + TMB sensing platform's feasibility for detecting Hg^{2+} was verified in actual water samples (industrial wastewater). The wastewater was determined to be free of Hg^{2+} by ICP-OES, so different concentrations of Hg^{2+} standard solutions (5, 10, and 30 μM) were added to the actual samples, which were then analyzed using the Pt/POP + TMB colorimetric platform. As shown in Table 1, the recoveries were in the range of 96.1%-107.4% with the relative standard deviations (RSD) of 1.97–2.28%, which indicated that the Pt/POP + TMB colorimetric platform has good accuracy and practicability for the determination of Hg^{2+} in actual water samples.

Removal of Hg^{2+}

The -S-R functional group in Pt/POP strongly bonds with mercury. In addition, Pt/POP has a large specific surface area and rich pore structure. The removal efficiencies (eq. S2) of Pt/POP were investigated with the initial concentrations of Hg^{2+} of 60, 70, 80, 90, and 100 ppm, respectively. Figure 6A showed the removal of Hg^{2+} by Pt/POP for

Table 1 Determination of Hg^{2+} in industrial wastewater

Sample	Detected (μM)	Spiked (μM)	Found (μM)	Recovery (%)	RSD (%, $n=3$)
Industrial wastewater	0	5	4.8 ± 0.1	96.1	2.05
	0	10	10.5 ± 0.2	105.3	1.97
	0	30	32.2 ± 0.7	107.4	2.28

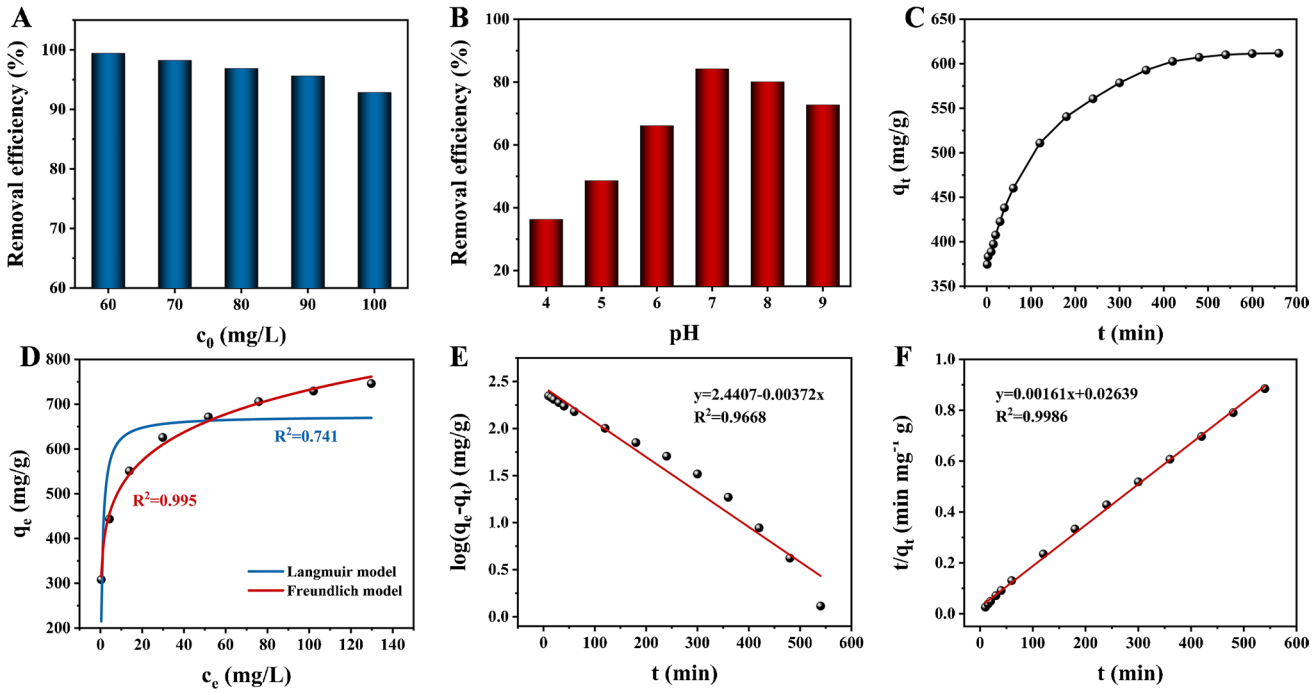

Fig. 6 **A** Performance of Pt/POP as an adsorbent for Hg^{2+} removal. **B** Removal efficiencies at different pH values. **C** Adsorption of Hg^{2+} as a function of time. **D** Equilibrium isotherms for Hg^{2+} adsorption by Pt/POP at room temperature. **E** Pseudo-first-order model fitting. **F** Pseudo-second-order model fitting

different concentrations of Hg^{2+} with the highest removal rate of more than 99.4%. The result indicated that Pt/POP is a promising adsorbent that can effectively capture Hg^{2+} from aqueous solution.

The pH of the aqueous Hg^{2+} solution (4–9) was adjusted using HNO_3 and NaOH, and the initial concentration of Hg^{2+} was 150 ppm. The highest removal efficiency was achieved at pH 7 (84.35%), as shown in Fig. 6B. The effect of contact time on the adsorption performance was also investigated. The adsorption capacity increased slowly with the increase of contact time and reached equilibrium within 8 h (Fig. 6C). The adsorption performance of Pt/POP was evaluated by studying the adsorption capacity of Pt/POP for Hg^{2+}. Equilibrium isotherms were measured for the adsorption of Hg^{2+} by the Pt/POP, and the equilibrium capacity (eq. S3) increased with increasing equilibrium concentration (Fig. 6D). The adsorption characteristics of Pt/POP were analyzed using Langmuir and Freundlich models (eq. S4-5). The fitted parameters were listed in Table S3, and the correlation coefficient of the Langmuir model was 0.741, and the isothermal data were more suitable for the Freundlich model ($R^2 = 0.995$). In addition, the Freundlich fitting results showed that the prepared Pt/POP was readily adsorbed, and the adsorption process was not uniform.

To better characterize the adsorption kinetics of Pt/POP on Hg^{2+}, pseudo-first-order and pseudo-second-order kinetic models (eq. S6-7) were used to fit the experimental data of q_t and t. As shown in Fig. 6E-F, the correlation coefficient of the pseudo-first-order kinetic equation was 0.9668, and the linear fit of q_t and t was more in line with the pseudo-second-order kinetic equation ($R^2 = 0.9986$), which indicated that the adsorption of Pt/POP on Hg^{2+} was mainly chemisorption. In addition, the adsorption capacity value ($q_{e,\,cal}$, 621.12 mg/g) calculated by the pseudo-second-order model was closer to the experimentally measured adsorption capacity ($q_{e,\,exp}$, 611.4 mg/g), further proving the accuracy of the pseudo-second-order kinetic model (Table S4).

Pt/POP was compared with other materials (Table S5). Compared with the bifunctional materials, although the detection limit of Pt/POP for Hg^{2+} was slightly higher, its adsorption capacity of Hg^{2+} was as high as 632.7 mg/g, demonstrating the superiority in adsorption performance. Moreover, the adsorption capacity of Pt/POP for Hg^{2+} was even higher than that of most adsorbents, mainly attributed to the abundant -S-R groups in Pt/POP, its inherent porosity, and large specific surface area. Therefore, Pt/POP, as a bifunctional nanocomposite, exhibits excellent potential for application in catalysis and adsorption.

Conclusion

POP was synthesized using pyrrole and BMTA as monomers, and then, Pt/POP was prepared by homogeneously immobilizing Pt NPs into the POP material. It was found that the oxidase-like activity of the Pt/POP-Hg^{2+} system was significantly increased 16-fold compared to the Pt/POP system. A colorimetric method for the detection of Hg^{2+} was developed based on the Hg^{2+}-enhanced oxidase-like activity of Pt/POP, which has the advantages of excellent selectivity, wide detection range, and rapidity, and satisfactory recoveries in the detection of Hg^{2+} in industrial wastewater. Meanwhile, Pt/POP, as an efficient adsorbent, showed potential application in removing Hg^{2+}. Nevertheless, the adsorption mechanism of Pt/POP on Hg^{2+} still needs to be explored more comprehensively and deeply so that we can understand its adsorption behavior more accurately. This work provides new ideas for the rational design of multifunctional nanomaterials, which will expand the application of nanomaterials in heavy metal detection and removal.

Supplementary Information The online version contains supplementary material available at https://doi.org/10.1007/s00604-024-06471-5.

Authors' contribution Liqin Zhu: Investigation, Data curation, Writing—original draft. Congcong Lou: Writing—review & editing. Xiaomei Zhang: Supervision, Writing—review & editing. Fei Yang: Project administration, Resources, Supervision, Writing—review & editing, Funding acquisition.

Funding This work was supported by the Natural Science Foundation of Shandong Province (No. ZR2021QB063).

Data availability All data generated or analysed during this study are included in this published article [and its supplementary information files].

Declarations

Ethical approval This research did not involve human or animal samples (not applicable).

Competing interests The authors declare no competing interests.

References

1. Song S, Li Y, Liu QS, Wang H, Li P, Shi J, Hu L, Zhang H, Liu Y, Li K, Zhao X, Cai Z (2021) Interaction of mercury ion Hg^{2+} with blood and cytotoxicity attenuation by serum albumin binding. J Hazard Mater 412:125158
2. Cappello T, Pereira P, Maisano M, Mauceri A, Pacheco M, Fasulo S (2016) Advances in understanding the mechanisms of mercury toxicity in wild golden grey mullet (Liza aurata) by ^{1}H NMR-based metabolomics. Environ Pollut 219:139–148
3. Zalups RK, Ahmad S (2004) Homocysteine and the renal epithelial transport and toxicity of inorganic mercury. J Am Soc Nephrol 15:2023–2031
4. Liu N, Cai X, Jia L, Wang X, Yuan W, Lin C-J, Wang D, Feng X (2023) Quantifying mercury distribution and source contribution in surface soil of Qinghai-Tibetan plateau using mercury isotopes. Environ Sci Technol 57:5903–5912
5. Hsu C-J, Chen Y-H, Hsi H-C (2020) Adsorption of aqueous Hg^{2+} and inhibition of Hg^{0} re-emission from actual seawater flue gas desulfurization wastewater by using sulfurized activated carbon and NaClO. Sci Total Environ 711:135172
6. Qin R, Chang S, Mei J, Hong Q, Yang S (2022) Selective removal of Hg^{2+} from acidic wastewaters using sulfureted Fe_2TiO_5: underlying mechanism and its application as a regenerable sorbent for recovering Hg from waste acids of smelters. Water Res 221:118796
7. Tang W, He M, Chen B, Ruan G, Xia Y, Xu P, Song G, Bi Y, Hu B (2023) Investigation of toxic effect of mercury on Microcystis aeruginosa: correlation between intracellular mercury content at single cells level and algae physiological responses. Sci Total Environ 858:159894
8. Kim YG, Kwon SY, Washburn SJ, Brooks SC, Yoon JW, Besnard L (2024) Reconsidering mercury sources and exposure pathways to bivalves: insights from mercury stable isotopes. Water Res 248:120843
9. Zhang L, Bi X, Liu X, He Y, Li L, You T (2023) Advances in the application of metal–organic framework nanozymes in colorimetric sensing of heavy metal ions. Nanoscale 15:12853–12867
10. Sanjabi S, Keyvan Rad J, Salehi-Mobarakeh H, Mahdavian AR (2024) Dual-chromic cellulose paper modified with nanocapsules containing leuco dye and spiropyran derivatives: a colorimetric portable chemosensor for detection of some heavy metal cations. J Environ Chem Eng 12:111724
11. Zhang X, Sun C, Li R, Jin X, Wu Y, Fu F (2023) Dual-loading of Fe_3O_4 and Pd nanoparticles on g-C_3N_4 nanosheets toward a magnetic nanoplatform with enhanced peroxidase-like activity for loading various enzymes for visual detection of small molecules. Anal Chem 95:5024–5033
12. Li B, Wu W, Lin J-M, Wang T, Hu Q, Yu L (2024) Water in liquid crystal emulsion-based sensing platform for colorimetric detection of organophosphorus pesticide. Food Chem 436:137732
13. Shi Y, Liu Z, Liu R, Wu R, Zhang J (2022) DNA-encoded MXene-Pt nanozyme for enhanced colorimetric sensing of mercury ions. Chem Eng J 442:136072
14. Li G, Wu Y, Zhong C, Yang Y, Lin Z (2023) Predesigned covalent organic framework with sulfur coordination: anchoring Au nanoparticles for sensitive colorimetric detection of Hg(II). Chin Chem Lett 35:108904
15. Liang L, Chen Q, Jiang F, Yuan D, Qian J, Lv G, Xue H, Liu L, Jiang H-L, Hong M (2016) In situ large-scale construction of sulfur-functionalized metal–organic framework and its efficient removal of Hg(ii) from water. J Mater Chem A 4:15370–15374
16. Yang L, Song Y, Li J, Xu W, Peng C, Wang L (2023) S, N-rich luminous covalent organic frameworks for Hg^{2+} detection and removal. Chemosphere 311:136919

17. Chowdhury A, Das SK, Mondal S, Ruidas S, Chakraborty D, Chatterjee S, Bhunia MK, Chandra D, Hara M, Bhaumik A (2021) Sulfur-containing nitrogen-rich robust hierarchically porous organic polymer for adsorptive removal of mercury: experimental and theoretical insights. Environ Sci Nano 8:2641–2649
18. Shan H, Li S, Yang Z, Zhang X, Zhuang Y, Zhu Q, Cai D, Qin P, Baeyens J (2021) Triazine-based N-rich porous covalent organic polymer for the effective detection and removal of Hg (II) from an aqueous solution. Chem Eng J 426:130757
19. Fan L, Zhou A, Zhong L, Zhang Z, Liu Y (2019) Selective and effective adsorption of Hg(II) from aqueous solution over wide pH range by thiol functionalized magnetic carbon nanotubes. Chemosphere 226:405–412
20. Xu X-Y, Yan B (2016) Fabrication and application of a ratiometric and colorimetric fluorescent probe for Hg^{2+} based on dual-emissive metal–organic framework hybrids with carbon dots and Eu^{3+}. J Mater Chem C 4:1543–1549
21. Zhang L, Jiao X, Zhang H, He S, Cheng X (2022) Novel chitosan–naphthalimide–amino acid fluorescent powder for selective detection and removal of Hg^{2+}/Hg^{+} and Fe^{2+} in aqueous solution. Chem Pap 76:7037–7049
22. Liang N, Ge X, Zhao Y, Xia L, Song Z-L, Kong R-M, Qu F (2023) Promoting sensitive colorimetric detection of hydroquinone and Hg^{2+} via ZIF-8 dispersion enhanced oxidase-mimicking activity of MnO_2 nanozyme. J Hazard Mater 454:131455
23. Ding Y, Liu T, Wang Q, Gu J, Li Y, Zhang Z, Wang X (2023) An enrichment-colorimetry integration strategy for nM-level Hg^{2+} detection in environmental waters based on an efficient Fe_7S_8-100 nanozyme and smartphone-based visual assay. Sens Actuators, B Chem 390:133995
24. Hu P, Liu B, Xia C, Zhu H, Wang M, Niu X (2023) Polyhedral MnSe microparticles with specific Hg^{2+}-suppressed oxidase-like activity: toward a green and low-cost turn-off method for Hg^{2+} detection. Sens Actuators, B Chem 382:133539
25. Zhao Y, Gui L, Chen Z (2017) Colorimetric detection of Hg^{2+} based on target-mediated growth of gold nanoparticles. Sens Actuators, B Chem 241:262–267
26. Khani H, Abbasi S, Tavakkoli Yaraki M, Tan YN (2022) A naked-eye colorimetric assay for detection of Hg^{2+} ions in real water samples based on gold nanoparticles-catalyzed clock reaction. J Mol Liq 345:118243
27. Lian Q, Liu H, Zheng X, Li X, Zhang F, Gao J (2019) Enhanced peroxidase-like activity of CuO/Pt nanoflowers for colorimetric and ultrasensitive Hg^{2+} detection in water sample. Appl Surf Sci 483:551–561
28. Deng H, He S, Lin X, Yang L, Lin Z, Chen R, Peng H, Chen W (2019) Target-triggered inhibiting oxidase-mimicking activity of platinum nanoparticles for ultrasensitive colorimetric detection of silver ion. Chin Chem Lett 30:1659–1662
29. Lu S, Hu Y, Wan S, McCaffrey R, Jin Y, Gu H, Zhang W (2017) Synthesis of ultrafine and highly dispersed metal nanoparticles confined in a thioether-containing covalent organic framework and their catalytic applications. J Am Chem Soc 139:17082–17088
30. Wang L, Wang J, Wang Y, Zhou F, Huang J (2022) Thioether-functionalized porphyrin-based polymers for Hg^{2+} efficient removal in aqueous solution. J Hazard Mater 429:128303
31. Sun Q, Aguila B, Perman J, Earl LD, Abney CW, Cheng Y, Wei H, Nguyen N, Wojtas L, Ma S (2017) Postsynthetically modified covalent organic frameworks for efficient and effective mercury removal. J Am Chem Soc 139:2786–2793
32. Yu W, Porosoff MD, Chen JG (2012) Review of Pt-based bimetallic catalysis: from model surfaces to supported catalysts. Chem Rev 112:5780–5817
33. Huang N, Zhai L, Xu H, Jiang D (2017) Stable covalent organic frameworks for exceptional mercury removal from aqueous solutions. J Am Chem Soc 139:2428–2434
34. Gao X, Li M, Zhao Y, Zhang Y (2019) Mechanistic study of selective adsorption of Hg^{2+} ion by porous alginate beads. Chem Eng J 378:122096
35. Li H, Liu H, Zhang J, Cheng Y, Zhang C, Fei X, Xian Y (2017) Platinum nanoparticle encapsulated metal-organic frameworks for colorimetric measurement and facile removal of mercury(II). ACS Appl Mater Interfaces 9:40716–40725